2. Бараненко В. И., Янченко Ю. А., Гулина О. М., Докукин Д. А. О расчете скорости эрозионно-коррозионного износа и остаточного ресурса трубопроводов АЭС. *Изв. вузов. Ядер. энергетика*. 2010. № 2. С. 55–63.
3. Милешкин М. Б., Библик И. В. Применение специального расчетно-экспериментального метода для оценки остаточного ресурса элементов конструкций по фактическому состоянию материала. *Надежность и долговечность машин и сооружений*. 2006. Вып. 27. С. 304–310.
4. Милешкин М. Б., Библик И. В., Инкулис В. В. Оценка вероятности безотказной работы оборудования АЭС на основе моделирования изменения степени эксплуатационной поврежденности. *Надежность и долговечность машин и сооружений*. 2009. Вып. 32. С. 105–112.
5. РД ЭО 0571-2006. Нормы допустимых толщин элементов трубопроводов из углеродистых сталей атомных станций. – Введ. 2006-11-01. – М.: ОАО «Концерн Росэнергоатом», 2006. 44 с.
6. Бараненко В. И., Гулина О. М., Докукин Д. А. Методологическая основа прогнозирования эрозионно-коррозионного износа оборудования АС методом нейросетевого моделирования. *Изв. вузов. Ядер. энергетика*. 2008. № 1. С. 3–8.
7. Бараненко В. И., Гетман А. Ф., Овчаров О. В., Гусаров А. Е. Использование программных средств для расчета коррозии трубопроводов и оборудования энергоблоков АЭС. [Электронный ресурс]. – Режим доступа: www.gidropress.podolsk.ru/files/proceedings/mntk2017/autorun/article19-ru.htm
8. Хайкин С. Нейронные сети: пер. с англ. – М.: Издат. дом «Вильямс», 2006. 1104 с.

UDC 539.3:629.7

DYNAMIC PROCESSES DURING THE THROUGH-PLASTIC-DAMPER SHOCK INTERACTION OF ROCKET FAIRING SEPARATION SYSTEM COMPONENTS

[1] Boris Zaytsev,
b.zajtsev@gmail.com

[1] Aleksandr Asayenok

[1] Tatyana Protasova,
tatyprotasova@gmail.com

[2] Dmitriy Klimenko

[2] Dmitriy Akimov,
AkimovDV@kbu.net

[2] Vladimir Sirenko

[1] A. Podgorny Institute of Mechanical Engineering Problems of NASU,
2/10 Pozharsky St., Kharkiv, 61046, Ukraine

[2] Yuzhnoye State Design Office,
3 Krivorozhskaya St., Dnipro, 49008, Ukraine

This article deals with the actual issues of ensuring the dynamic strength of rocketry components using pyrotechnics. It studies the shock interaction of rocket fairing pyrotechnic separation system components during the second phase of the system operation at so-called capturing. The contacting of the system components occurs through a viscoelastic damper. The damper is installed between a movable part and a fixed one to 'attenuate' impact due to plastic deformation. The damper acts as a one-way connector – it limits compression and does not prevent separation. The whole structure is assumed to be elastic, and plastic deformation is concentrated in the damper. The mechanical model is represented as a combination of elastic elements and a nonlinear damper. The technique of taking into account the nonlinearity of a damper is based on the introduction of variable boundary forces on the damper ends. In the case of plastic compressive deformations, boundary forces increase the deformation, restrained by elastic forces, and when the contact disrupts (separation), they completely compensate the stresses in the damper model, nullifying them. A three-dimensional computational model of the fairing assembly composite design is constructed. The damper is presented in the form of a continuous thin ring. The finite element method is used. The calculation of the structural dynamics with respect to time is carried out by the Wilson finite-difference method. Verification of the technique on the test problem with the known wave solution is carried out. Calculation studies of the dynamic stress state at different impact speeds for damper variants with different plastic stiffness are performed: steel elastic (damper without holes, 'rigid', for comparison); initial (damper with holes, plastic, soft) and rational (damper with a selected characteristic of rigidity). It is shown that the initial damper is inefficient due to insufficient rigidity. The characteristics of plastic stiffness are determined, under which dynamic stresses are significantly reduced in relation to the initial structure. The maximum dynamic stresses in the pyrotechnic separation system of the fairing with rational dampers strongly depend on the impact speed. At significant speeds, they exceed the plasticity limit. A more precise formulation of the 'catch-up' task should be carried out taking into account the plasticity in the entire structure.

Keywords: *fairing, separation system, impact, stress, contact, damper, plasticity.*

Introduction

Fairing separation is a complex and responsible part of a rocket flight mission, performed by a separation system (SS). In rocket production, various SS designs are used [1, 2], but the most widespread systems are of pyromechanical and detonation types. The use of pyrotechnic devices in SSes causes the emergence of intense loads of a shock-pulse character, which increases the actuality of ensuring dynamic strength. The fairing is not used after separation, so during the process of separation, irreversible processes in the propulsion elements, associated with plastic deformation or microfracture, can be allowed. At that, the main task is to preserve the functionality of the fairing separation system. Prediction of SS strength without restriction on deformation in the elastic region also contributes to the improvement of mass indices and allows using damping devices with plastic elements.

In calculating the strength of fairings, quasistatic state models are mainly used without taking into account the dynamics of separation processes [3, 4]. The dynamic processes in the elastic deformation region during separation are investigated in [5–7] for fairings and in [8, 9] for spacecraft and launch vehicles (LV). Studies in the field of structural dynamics during fairing separation, taking into account physical nonlinearity, are presented insignificantly.

Fairing separation system structure and its functioning. Strength issues and problem formulation

The subject of the study is the mechanical processes taking place during the operation of a ready-assembled fairing pyrotechnic separation system (FPSS) shown in figure 1.

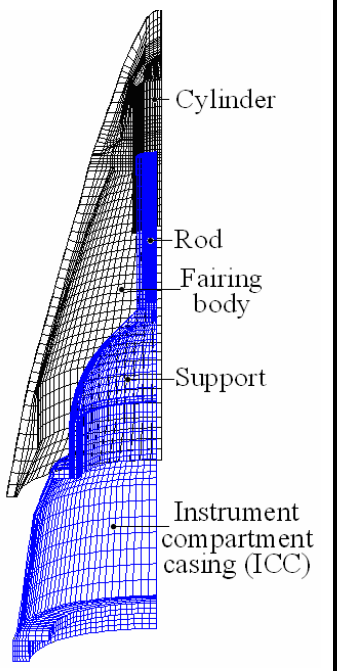

Fig. 1. FPSS general scheme

The separation system consists of two large components that make up a movable part (MP) and a fixed part (FP). The FP includes a support and a connected rod (piston), which are supported by an instrument compartment casing (ICC) and pyrobolted to it in transport position. The movable part includes a cylinder and a connected fairing body. The rod and cylinder form a movable pair and can move relative to each other, the closed space that they form, changing its volume. Inside the rod-cylinder pair volume, pyrotechnics (powder) is placed, which, during combustion, creates pressure, under which the cylinder, and with it the entire movable part, move rapidly relative to the fixed part, increasing the speed and accumulating kinetic energy. The FPSS pyrotechnics includes pyrobolts and powder, which are triggered in a certain sequence. First, the pyrobolts are triggered and the power connection between the support (FP) and ICC is eliminated, and then the powder is ignited and MP is set in motion. Several phases can be identified in FPSS operation, the first of which is the displacement of the cylinder from the initial position to the final one. In the final position, free relative displacement is impossible, and a power contact occurs between the rod and cylinder, which determines the second phase of FPSS operation, the so-called 'catch-up'. The 'catch-up' results in equalizing MP and FP speeds, i.e. combining them into a single structure, and the possibility to separate from the rocket owing to the additional speed relative to it. The third phase of FPSS operation begins at the moment of 'catch-up', when a side nozzle opens and a reactive jet of leaking powder gases arises, resulting in the fairing lateral drift-away from the rocket trajectory.

To partially solve the problem, it is supposed to use additional collision-softening elements in the form of dampers, whose purpose is to prolong the process of speed equalization and, consequently, reduce the dynamic strength of the structures. At that, a complex behavior of the structures interacting through the damper is possible, which manifests itself as contacting, or its interrupting, i.e. rebound. At considerable collision speeds, plastic deformations can develop in the structures, which considerably impedes the solution to the problem. To simplify it, the structures are assumed to be elastic when colliding, allowing the possibility of the damper being plastically deformed and the structures being separated.

In this case, there arises the problem of choosing the damper characteristics for plastic deformation, determined by its design factors and the material used, under which the dynamic stresses during the whole process of shock interaction are minimal. It should be noted that the loss of kinetic energy (speed after separation) due to the irreversible work of the damper plastic deformation should also be minimal.

Research technique and FPSS design model

The technique is based on the application of the finite element method (FEM) in a three-dimensional setting, where a volumetric multilinear finite element with a topologically regular discretization system is used. When modeling the material of the structural elements, continuous heterogeneity or piecewise homogeneity and the presence of curvilinear anisotropy are allowed, which makes it possible to compute complex and composite structures.

The application of the FEM procedure based on the use of the Lagrange-d'Alembert kinetostatic variational principle leads to a mathematical model represented by a system of ordinary differential equations [10]

$$[\mathbf{M}]\ddot{u} + [\mathbf{D}]\dot{u} + [\mathbf{K}]u = F_e, \quad (1)$$

where u is the displacement vector of the finite element (FE) grid nodes; F_e is the vector of a given load varying in time; **[M], [D], [K]** are the mass, damping and strength matrices, respectively.

It is to be noted that in dynamical problems with impulse action, where the process is studied during a relatively short time interval, the damping effect is insignificant. In addition, the damping values are either generally unknown or determined with little accuracy. Therefore, the damping effect in this work is not taken into account ([D]=0).

The solution to the matrix equation (1.1) is implemented using the implicit Wilson finite-difference scheme [11], which is absolutely stable, of the second order of accuracy. According to this scheme, the acceleration at the time step Δt is a linear function, and the equations (1) are written for the point of time $t+\theta\Delta t$ (θ=1.4). There is no restriction on the choice of the step Δt which is determined mainly by the requirement to the accuracy and efficiency of calculations. The finite-difference analogue of the equation (1) can be written in the form

$$[\hat{\mathbf{K}}]u_{t+\theta\Delta t} = \hat{R}_{t+\theta\Delta t}, \quad (2)$$

where $[\hat{\mathbf{K}}]$ is the modified strength matrix; $\hat{R}_{t+\theta\Delta t}$ is the modified right-hand side (vector of external forces); $u_{t+\theta\Delta t}$ – is the displacement vector for the point of time $t+\theta\Delta t$.

The displacements $u_{t+\Delta t}$, velocities $\dot{u}_{t+\Delta t}$, and accelerations $\ddot{u}_{t+\Delta t}$ at the end of the step (the point of time $t+\Delta t$) are determined using the finite-difference formulas including the values of the previous step kinematic parameters $u_t, \dot{u}_t, \ddot{u}_t$ and the displacement values $u_{t+\theta\Delta t}$ [11].

Problem statement with regard to studying the dynamics of FPSS components during 'catch-up' has a specificity that is related to the absence of fixations. At that, oscillation processes are excited in the constructions, accompanied by the former displacement in space as a solid body. Of special importance is also the formulation of the 'catch-up' problem, where the structure colliding components are considered as a whole, but they have different initial speeds, i.e. the right-hand side in the equation (1) is zero, and the perturbation of the system is formed by specifying discontinuous initial conditions.

The computational model of the colliding FPSS components during the 'catch-up' is shown in figures 2, 3, where the fixed component (the support and rod) and the movable component (the cylinder and fairing body) moving at a speed V_0, contact through the damper, whose location is shown in more detail in figure 3, a. The damper is presented as a solid cylindrical ring with the geometrical parameters of the initial damper construction (height L=10 mm, thickness h=3 mm), whose characteristic at compression is determined by the stiffness diagram $N(\lambda)$, where $\lambda = u_y(A) - u_y(B)$ is the relative displacement of the damper ends (shortening under compression); N is the current axial thrust transmitted through the damper. The characteristic values of the relative motion of λ are the initial plastic displacement λ_p, at which the damper plastic deformation begins, and the limiting plastic displacement λ_{lim} ($\lambda<\lambda_{lim}$), at which plastic deformation is impossible. The change in the force $N(\lambda)$ during plastic deformation is a characteristic of the damper construction plastic stiffness at a given value of λ and it is determined by the instantaneous yield strength of the damper material and its

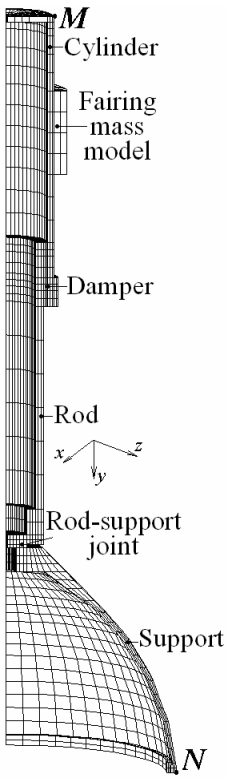

Fig. 2. Fairing separation system complex structure model at 'catch-up'

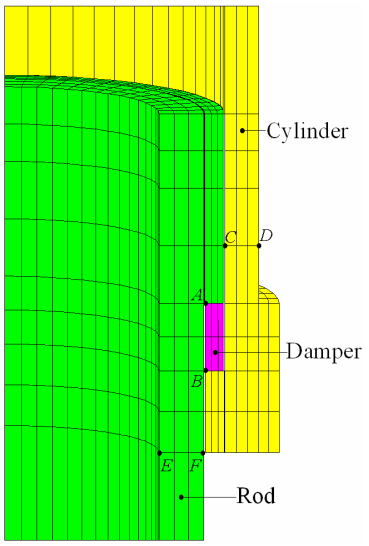

a

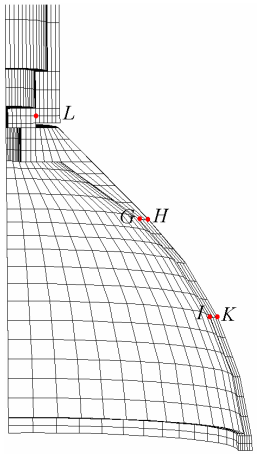

b

Fig. 3. Damper location:
a – model; b – the data read-out points

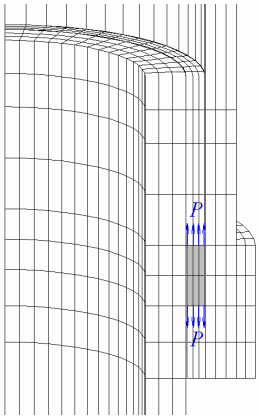

Fig. 4. Diagram of introducing boundary forces on damper ends

geometric parameters – height and cross-sectional area. For a material with hardening, the dependence $N(\lambda)$ is variable, and for an ideal elastic-plastic material the force N reaches the limiting value N_p, i.e. the load-bearing capacity of the structure in the plastic state, and remains so when deformed. The power contact of the damper with the support and rod, and, accordingly, the transfer of forces are carried out on the ends, i.e. there is a gap between the cylindrical surfaces of these parts. The damper only works in compression and carries out one-waycommunication, allowing the separation of the parts contacting through it. ICC is not included in the design model, since there is practically no power connection between the support and ICC after the destruction of the pyrobolts. The fairing body in the model is considered as a solid one of the same mass. Fig. 2 also shows the location of the points for which the results of the calculations of displacements, velocities, and stresses are presented.

The damper plastic stiffness diagram $N(\lambda)$ in the computational studies of FPSS dynamics allows for variation. This corresponds to the damper design modification, which, in principle, can be considered as a complex system consisting of a series of elements with their own properties, whose combination can affect the diagram $N(\lambda)$.

For example, for a damper of the initial structure in the form of a short cylindrical shell with a large number of radial holes, the plastic deformation diagram $N(\lambda)$ has been obtained approximately. Simplified models of damper drafting were used – kinematic ones, taking into account the flattening of the holes and the model of plastic hinges. A much more accurate and coherent determination of the diagram $N(\lambda)$ is connected with the solution to an elastic-plastic problem with large deformations, taking into account the contacting of hole boundaries, which is practically impossible because of the difficulties in realization. The diagram $N(\lambda)$ can also be obtained experimentally. The calculation results of the $N(\lambda)$ diagram points for the initial damper are as follows: relative displacements λ_i: λ_0=0, λ_1=0,015 mm, λ_2=3 mm, λ_3=6 mm, $\lambda_4=\lambda_{lim}$=8 mm; loads N_i: N_0=0, N_1=30 kN, N_2=60 kN, N_3=103 kN, N_4=316 kN.

To evaluate the collisional damping effectiveness of FPSS components during 'catch-up', a justification is necessary with the help of computational simulation. In calculating the dynamics of contact shock interaction, the approach is used, according to which all the FPSS composite design components are considered to be elastically deformable, and in order to take into account the nonlinear behavior of the damper, associated with plastic deformation or breaking the contact, the method of introducing boundary variable forces is applied, whose arrangement is shown in figure 4.

The boundary forces P refer to external forces, are recalculated at each step of integration over time, and are included into the expression $\hat{R}_{t+\theta\Delta t}$ of the right-hand side of (2). Their purpose is to compensate for the elastic forces that are developing in the damper model that is part of the design as an elastic element. At plastic compressive deformations, the forces P must increase the deformation, restrained by elastic forces, and in the case of contact failure, i.e. the elements separating from each other, the boundary forces must completely compensate for the stresses in the damper model by zeroing them. The scheme for determining the boundary forces for different damper states – active plastic deformation, unloading or separation – is shown in figure 5.

The state of a damper as a one-dimensional element with nonlinear behavior is determined by the relative motion of its ends. At that, various mechanical states are possible: active plastic deformation, unloading that takes place according to the elastic law, and separation of contact elements from each other. An evaluation of the damper state is performed at each time step, respectively, according to which the boundary forces P are calculated.

In the case of elastoplastic deformation, both elastic λ_e and plastic λ_p components can be distinguished from the total relative displacement λ in figure 5

$$\lambda = \lambda_e + \lambda_p .$$

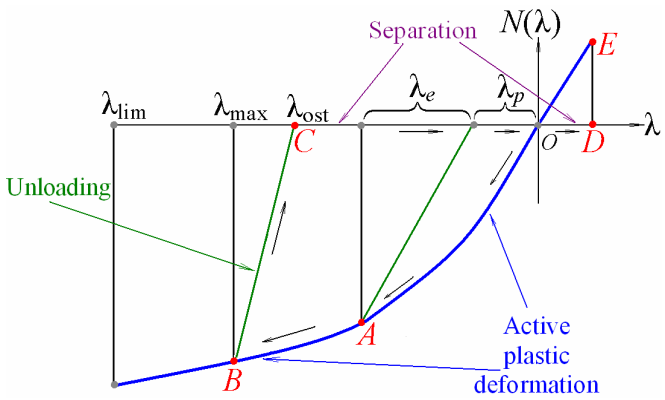

Fig. 5. Scheme for determining the boundary forces P at damper plastic deformation, elastic unloading, and separation

The plastic component λ_p can be considered as an additional component and taken into account in the law of elasticity by the method of additional deformations [12]. Its definition is performed by iterations, when the elastic problem is being solved, and reduces to the introduction of additional volume forces, which are brought to the nodes of the finite elements on the damper ends [13], i.e. to the boundary forces P. The boundary forces P are proportional to the plastic component λ_p

$$P = E\lambda_p L^{-1} .$$

Given that $\lambda_p = \lambda - \lambda_e$, and λ_e is a known function of the current value of the relative displacement $\lambda_e = \lambda_e(\lambda)$, we get

$$P = E\,L^{-1}[\lambda - \lambda_e(\lambda)]. \tag{3}$$

At the step of integration with respect to time, the displacements are determined, taking into account the boundary forces, by the relation

$$\lambda = \lambda_0 + \alpha P , \tag{4}$$

where λ_0 is the displacement determined from (2), without taking into account the boundary forces; α is the displacement at a step from the momentum of unitary boundary forces.

The equations (3), (4) constitute a system relative to λ, P. Excluding P, we obtain a nonlinear equation for λ, whose solution is performed by iterations

$$\lambda = \frac{\lambda_0 + \alpha E L^{-1}\lambda_e(\lambda)}{1 - \alpha E L^{-1}} \tag{5}$$

The denominator in (5) is different from zero, since the term $\alpha EL^{-1} < 1$ is the compliance ratio from the action of the boundary forces at both the dynamic (α) and static ($E^{-1}L$) loads. It is obvious that under dynamic loading, when the system inertia exerts influence, the compliance is lower.

The state of active plastic deformation takes place when the inequality is satisfied (without taking into account the displacement sign)

$$\Delta\lambda_p = \lambda_p^{i+1} - \lambda_p^{i} > 0 , \tag{6}$$

where λ_p^i, λ_p^{i+1} are the plastic components of the displacement at steps i, i+1, respectively.

The state of the damper is characterized by the position of the point on the plane λ, N. For the active plastic deformation, the point lies on the curve $N(\lambda)$ (Fig. 5), and the boundary forces in this case are determined from the relation

$$P = \frac{[\lambda_0 - \lambda_e(\lambda)]L^{-1}E}{1 - \alpha EL^{-1}} .$$

If the inequality (6) is not satisfied, then the state of elastic unloading is fixed, at which the plastic component is considered to be fixed and equal to the reached maximum value, and, accordingly, the boundary forces are also fixed

$$P = EL^{-1}\left[\lambda_{\max} - \lambda_e(\lambda_{\max})\right],$$

where $\lambda_{\max}$ is the achieved maximum value of the relative displacement (point *B*, Fig. 5).

The unloading occurs under the condition $\lambda > \lambda_{ost}$ (Fig. 5), where $\lambda_{ost} = \lambda_{\max} - \lambda_e(\lambda_{\max})$, and when it is violated, the state is defined as a separation, in which there is no force interaction of the elements through the damper. The magnitude of the boundary forces necessary for simulating this state is determined from the condition $\lambda_e = 0$, which leads to the relation

$$P = \frac{\lambda_0 L^{-1} E}{1 - \alpha E L^{-1}}.$$

In the state of separation at negative λ, the boundary forces $P < 0$ (the damper compression, *CO* section in figure 5, and at positive λ – $P > 0$ (the damper extension, *OD* segment in figure 5.

The proposed technique has been tested, in particular for the impact contact of solids through an elastic-plastic element, the results of which are confirmed both qualitatively and quantitatively. Certain requirements are imposed on the accuracy of determining the unitary boundary forces, which are made to the strictness of correspondence to a given magnitude and equilibrium. At contact deformation, this has no significant value, but in the case of contact absence, at free movement, it does exert influence, introducing errors.

Evaluation of the technique accuracy from the example of a longitudinal impact

Calculations of shock processes have specificity, which manifests itself in the appearance of deformation waves, their interaction both with the boundary and with each other. To evaluate the possibility of reproducing wave processes, the techniques used need to be verified on problems with exact or known solutions. Here, we consider a solution to the problem with regard to the rod end longitudinal impact by a moving load.

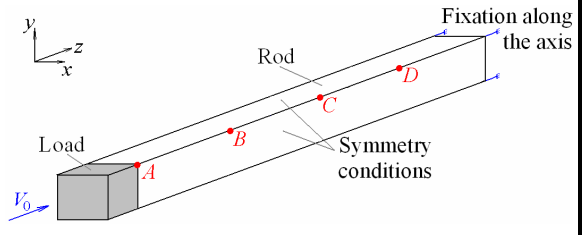

Fig. 6. Model of a moving load impact on the rod

The computational model of the problem with regard to the rod being impacted by a load of mass *M* moving with a speed V_0 is shown in figure 6, where the simulated rod is shown with the following parameters: length l=80 cm, material density ρ=8 g/cm^3, cross-section 2×2 cm, E=200 GPa, ν=0.3 at the mass ratio of the load and rod $\alpha = l\rho/M$=0.5. In the three-dimensional finite element model, discretization was used: in length – 80 FEs, in cross- section – one or three FEs, and one fourth part of the rod was considered with the setting of the symmetry conditions. The figure also shows the location of the control points, for which the numerical results are given below.

Impact simulation in the calculations is as follows. The load and rod are combined and considered within the framework of a general FE model. At that, one of FEs at the rod edge is considered to be a load, and its mechanical characteristics are accepted as high, which practically corresponds to an absolutely solid body. When setting the initial conditions, the speed of the load FE nodes is equal to V_0, and the nodes of the rest of the body are fixed. This approach physically corresponds to the conditions of contact between the load and rod at the moment of contact. The impact causes the appearance of elastic waves in the rod and its joint movement with the slowing load. After a certain time, the contact of the load with the rod is lost, that is, the load separates from the rod. Depending on the duration of the contact, which depends on the mass ratio of the load and rod, the number of wave passes along the rod can be different. The singularity of the wave process in this problem is the reflection of the wave from the load, which is equivalent to the reflection from a rigid sealing, in which the type of wave does not change (compression wave), but the stress at reflection increases abruptly.

Figures 7 to 9 respectively present the results of calculations of displacements and velocities at the rod points shown in figure 6, as well as the change in the rod stress at the point located near the load. The kinks in the displacement graphs and the jumps in the speed graphs correspond to the moments of the pas-

sage of the waves reflected from the rod ends. In the calculations, the speed discontinuities, when the front passes are manifested in the form of bursts and oscillations.

In the three-dimensional finite element model, transverse displacements due to the connection of deformations ($\nu \neq 0$) are taken into account as well. When the front passes, the transverse oscillations are excited, accompanied by shifts, whose magnitude is small, and it does not prevent part of the energy of the longitudinal oscillations from being lost. Consequently, the dynamic process becomes more complex and different from the assumptions in the core theory, with which the results are compared. To eliminate this effect, the calculations were carried out with a zero Poisson's ratio, at which the transverse oscillations did not arise, i.e. the calculated FE model was more consistent with the conditions adopted in the core model.

The main value by which the comparison was made in the problem under consideration is the time variation in the rod stress at the point of contact with the load, i.e., in fact the contact stress. The criterion for loss of contact between the load and rod is the change in the stress sign, and the point of time, when this occurs, determines the contact time. The comparison was made both with regard to stresses for the points of time t_1, t_2, t_3 (points *A, B, C* in figure 9) of the arrival of reflected waves to the load and impact duration, whose results are given in table 1. The stress of the load at the initial point of time according to the core theory is determined by the formula $\sigma_0 = V_0\sqrt{E\rho}$ .The calculated impact duration corresponded to the data of [14] with high accuracy.

Conclusions on the comparison of the calculated data, obtained by the method used, and data from [14] indicate the applicability of the developed software to solving problems with shock-pulse loading.

Results of computational simulation

The presented technique was used in calculations of shock interaction in FPSS components during 'catch-up' at various initial speeds of MP – 40; 60; 80 m/s and various dampers. The calculations were carried out for the damper of the original design, which, within the permissible plastic deformation, has small stiffness, as well as (for comparison) for a steel damper in a state of elasticity, where stiffness is high. In addition to these initial variants, research was conducted on rational variants of a damper characterized by the rigidity of an ideally elastic-plastic material, in which the dynamic tension of the construction is minimal. The limiting stiffness characteristics of dampers, i.e. their carrying capacity, in relative values $N_p^* = N_p/N_{st}$, where N_{st} is the magnitude of the longitudinal force from the maximum internal pressure ($N_{st} \approx 590$ kN), depend on the speed V_0 and take the following values: $N_p^* = 0.43$ (at $V_0 = 40$ m/s), $N_p^* = 1.4$ (at $V_0 = 60$ m/s), $N_p^* = 2.4$ (at $V_0 = 80$ m/s).

The results of computational studies for the displacements and speeds at reference points *A* and *B* (see figure 3,a) are presented in figures 10 and 11, and those for the stresses at reference points *C*, *F*, and *G* are presented both in figure 12 and in tables 2 to 4.

Characteristic of the interacting structures is the initial approach, accompanied by plastic deformation, followed by the unloading of a damper with subsequent disruption of contact and free movement of non-connected structural components. For an elastic steel damper, the draft upon contact is very low (figure 10), and if plastic properties are taken into account both in the initial and rational variants, it is high. A limitation was imposed on the limiting damper draft at compression, determined by λ_{lim} ($\lambda_{lim} = 8$ mm), the maximum draft values for the rational variants λ either being close to λ_{lim} or reaching it for

Table 1. Stresses σ/σ_0 in the rod near the load during wave passage

Point	Data 14]	FEM calculation
A	1.00	1.07
B	2.36	2.51
C	2.14	2.12

Table 2. Maximum values of the stress intensity in FPSS components at a speed V_0=40 m/s

Damper	$\sigma_{i\,\max}(C)$	$\sigma_{i\,\max}(F)$	$\sigma_{i\,\max}(G)$
elastic	1,68	1,27	1,45
initial	1,25	0,84	0,77
rational	0,67	0,37	0,37

Table 3. Maximum values of the stress intensity in FPSS components at a speed V_0=60 m/s

Damper	$\sigma_{i\,\max}(C)$	$\sigma_{i\,\max}(F)$	$\sigma_{i\,\max}(G)$
elastic	2,51	1,91	2,17
initial	2,23	1,63	1,66
rational	1,45	0,81	0,83

Table 4. Maximum values of the stress intensity in FPSS components at a speed V_0=80 m/s

Damper	$\sigma_{i\,\max}(C)$	$\sigma_{i\,\max}(F)$	$\sigma_{i\,\max}(G)$
elastic	3,35	2,54	2,89
initial	3,06	2,27	2,52
rational	2,09	1,30	1,39

a short time. This is due to the fact that for the greatest effect of reducing stresses, the equalization of velocities should occur over a longer period of time, and, accordingly, on a greater relative displacement of the damper ends. At that, the exhaustion of the deformation capacity ($\lambda=\lambda_{lim}$) should not be prolonged, since an additional shock effect will occur. The contact disruption occurs at the beginning of the reduction of the maximum compression achieved by the damper, in particular, when the displacement value λ_{lim} is deviated.

It can be noted that, as the impact speed V_0 increases, the speed equalization time (figure 11) for the rational variants decreases, which is associated with an increase in the recommended stiffness.

Data on the dynamic stresses in different FPSS components (point C – cylinder, point F – rod, point G – support) for different damper variants of are represented in figure 12, which shows the distribution of stress intensity over time, and in tables 2 to 4 its maximum values are given at different impact speeds. Stresses are represented in the relative values $\sigma^*_{i\max} = \sigma_{i\max} / \sigma_p$, where σ_p is the steel plasticity limit of the separation system components: cylinder, rod, and support (σ_p=1300 MPa).

The stress change in the variants of the initial and steel elastic dampers is similar in both magnitude and law of variation. The initial damper has small stiffness, which greatly reduces the compression force. Such a damper has almost no resistance and only postpones the moment of hard collision of its parts, which is typical for a steel elastic damper. The directional search for rational stiffness at various collision velocities of FPSS components has made it possible to significantly reduce the magnitude of the maximum dynamic stresses and, for some cases, introduce the structural components into the elastic stage of deformation.

It can be stated that the level of developed dynamic stresses is strongly dependent on the magnitude of the impact speed. At that, in order to obtain a rational design, the necessary plastic stiffness of the damper also increases strongly with increasing speed V_0. This is in correlation with an approximate estimate of the strength of the interaction of two solid bodies upon an absolutely inelastic impact, at which the speed equalization time is determined by the initial speed, and the force itself is assumed to be constant. According to such an estimate, the magnitude of the force depends quadratically on impact speed.

The calculations show that even for the rational designs of dampers, with increasing impact speed, plastic deformations can appear in FPSS components. The formulation of the problem used in this paper assumes the elastic behavior of the structural components and plastic behavior of a damper. It can be assumed that the plasticity in all the components also damps shock interaction, and, if taken into consideration, allows designing FPSSes in the field of plastic destruction. The clarification of the problem statement in this respect is the subject of further research.

Conclusions

1. The proposed technique for calculating the shock interaction of FPSS components through a damper, taking into account its plasticity and disruption of communication between the contacting components, has undergone testing and confirmed its efficiency.

2. It is shown that a directional change in the plastic stiffness of a damper can significantly affect the level of dynamic stresses in FPSS components. Different values of the limiting stiffness of a damper are determined by its design parameters (thickness, height) and the yield strength of the material.

3. An initial damper is inefficient due to insufficient rigidity. The intensive shock interaction through an initial damper with the appearance of high dynamic stresses shifts in time and is analogous to the case of a rigid damper (steel elastic damper).

4. For various impact speeds, rational parameters of the limiting plastic stiffness of a damper are determined, under which the maximum values of dynamic stresses in FPSS composite structure are minimized. The values of the stiffness parameters of rational dampers are different for different impact speeds and increase with increasing speeds. The time for the equalization of speeds upon collision decreases with the increase in the impact speed.

5. The maximum dynamic stresses in FPSSes with rational dampers strongly depend on impact speed and at significant velocities exceed the plasticity limit. A more precise formulation of the 'catch-up' task should be carried out taking into account the plasticity in the entire structure.

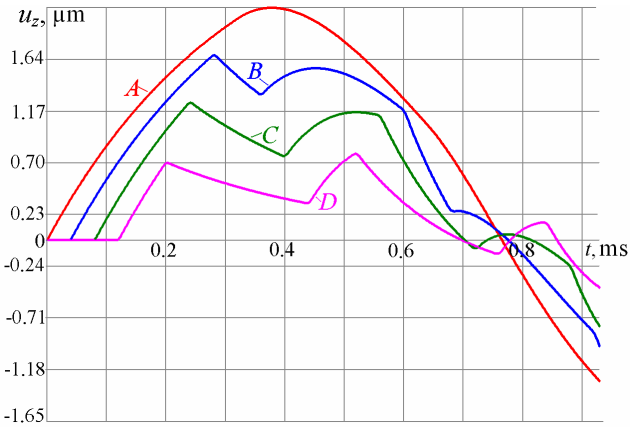

Fig. 7. Axial displacements at different points along the rod length

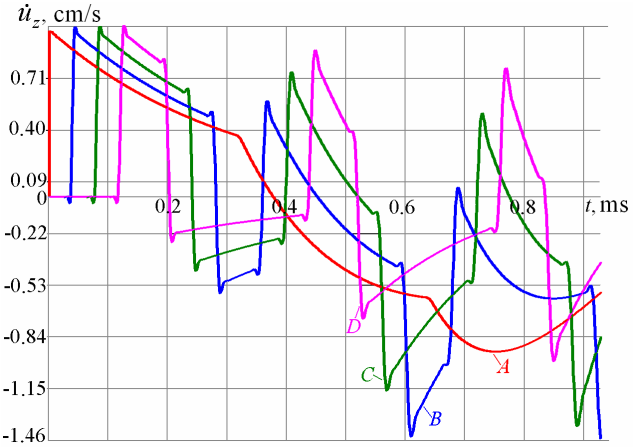

Fig. 8. Velocities along the rod axis at points along its length

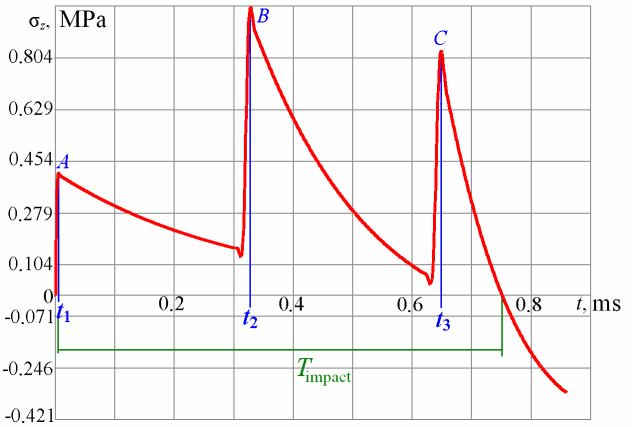

Fig. 9. Axial stress in the rod near the load

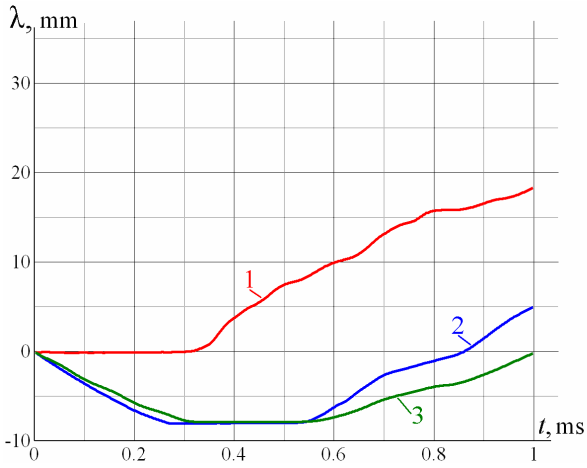

a

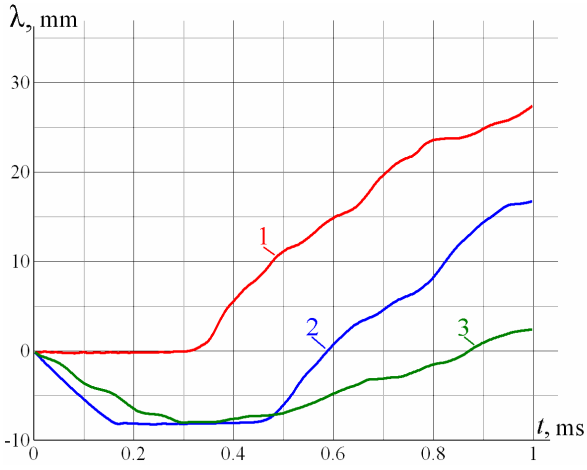

b

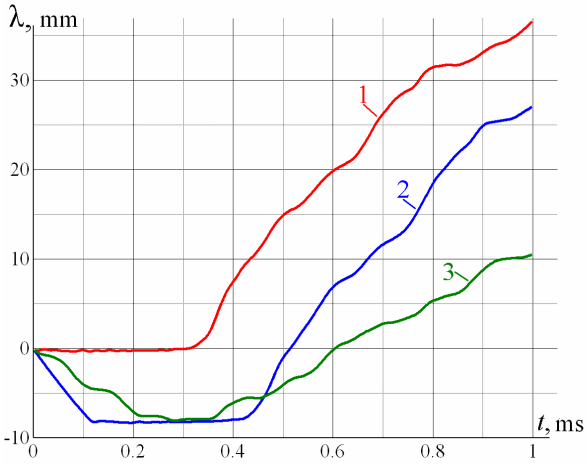

c

Fig. 10. Distance change between damper ends (points A, B):
a – V_0=40 m/s; b – V_0=60 m/s; c – V_0=80 m/s
1 – elastic damper; 2 – initial damper; 3 – rational damper

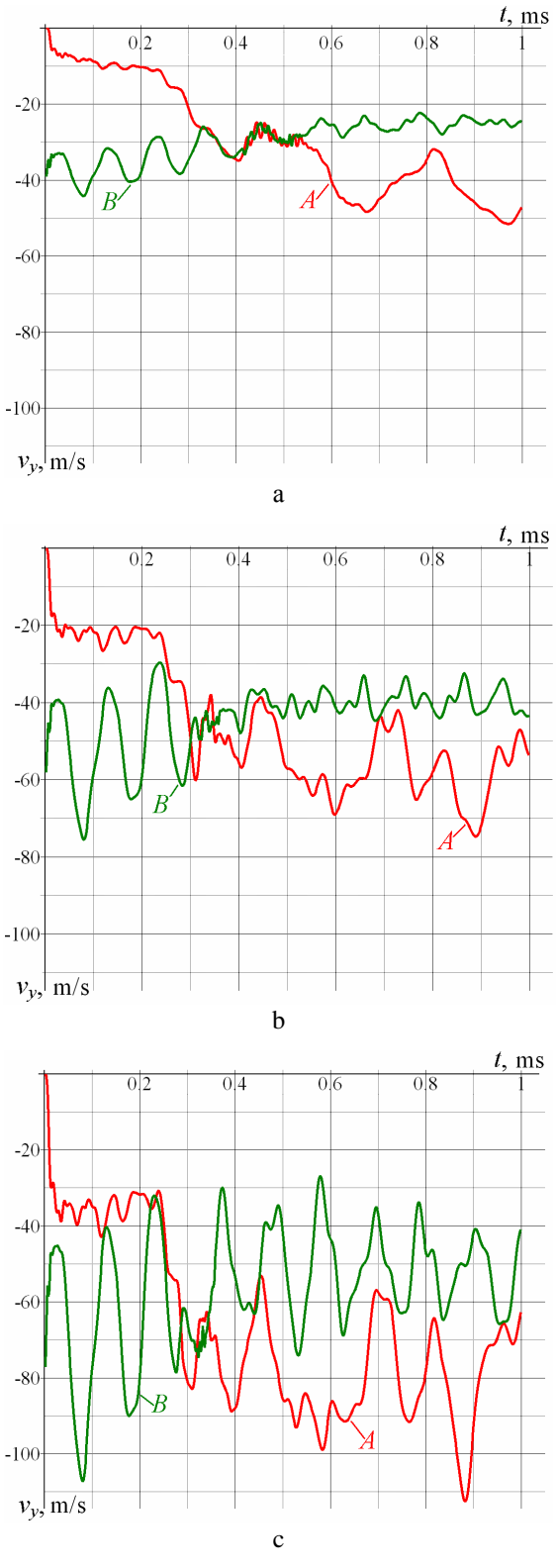

Fig. 11. Speeds of rational damper ends (points A, B):
a – V_0=40 m/s; b – V_0=60 m/s; c – V_0=80 m/s

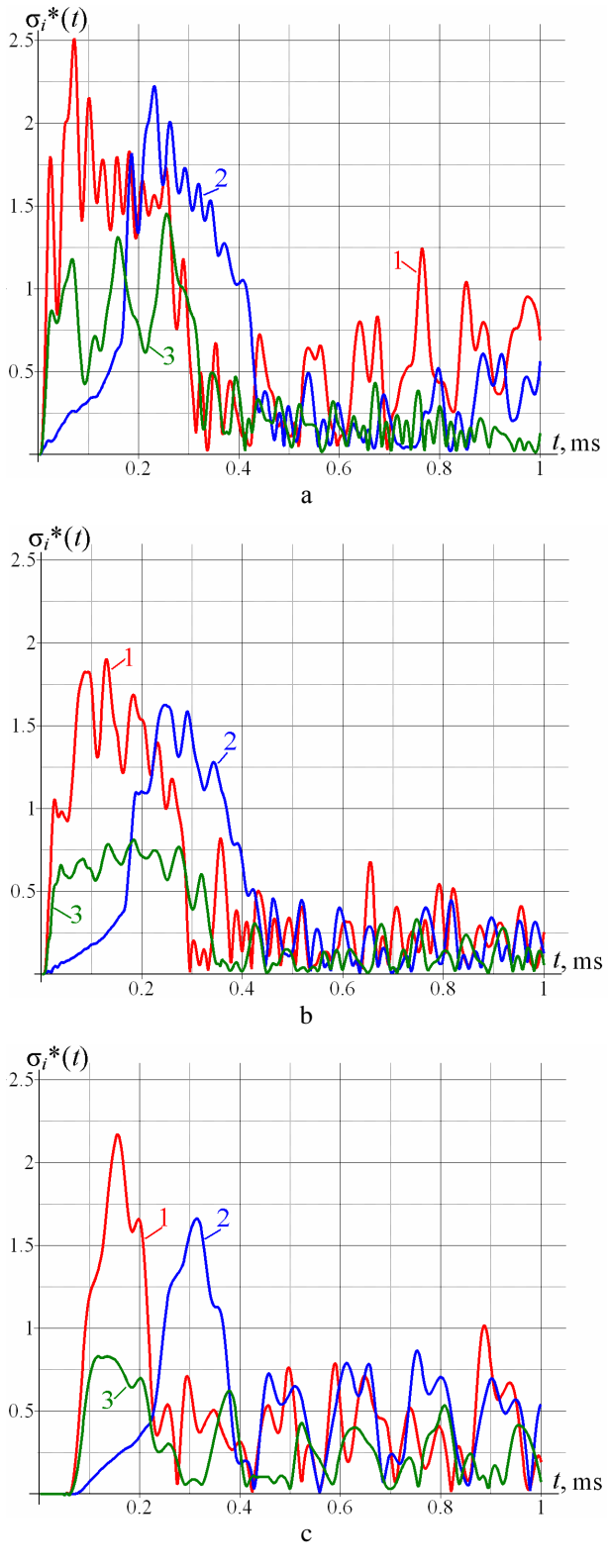

Fig. 12. Relative values of stress intensity at reference points at V_0=60 m/s:
a – point *C*; b – point *F*; c – point *G*
1 – elastic damper; 2 – initial damper; 3 – rational damper

References

1. Potapov, A. M., Kovalenko, V. A., & Kondratyev, A. V. (2015). *Sravneniye golovnykh obtekateley sushchestvuyushchikh i perspektivnykh otechestvennykh raket-nositeley i ikh zarubezhnykh analogov* [Comparison of head fairings of existing and promising domestic carrier rockets and their foreign counterparts]. Aviats.-kosm. tekhnika i tekhnologiya – Aerospace Technic and Technology, no. 1 (118), pp. 35–43 [in Russian].
2. Rusin M. Yu., Romashin, A. G., & Kamnev, P. I. (2004). *Opyt razrabotki golovnykh obtekateley letatelnykh apparatov* [Experience in development of head fairings for flying vehicles]. *Aviats.-kosm. tekhnika i tekhnologiya – Aerospace Technic and Technology*, no. 5(13), pp. 63–69 [in Russian].
3. Mossakovskiy, V. I., Makarenkov, A. G., Nikitin, P. I., & Savvin, Yu. I. (1990). *Prochnost raketnykh konstruktsiy: Ucheb. posobiye* [Strength of rocket structures: Training manual. B. I. Mossakovskii (Ed.). Moscow: Vysshaya shkola, 359 p. [in Russian].
4. Kolesnikov, K. S., Kokushkin, V. V., Borzykh, S. V., & Pankova, N. V. (2006). *Raschet i proyektirovaniye sistem razdeleniya stupeney raket: Ucheb. posobiye* [Calculation and design of separation systems of rocket stages: Training manual]. Moscow: Izd-vo MGTU im. N. E. Baumana, 376 p. [in Russian].
5. Konyukhov, A.S. (2014). *Opredeleniye zhestkostnykh i inertsionno-massovykh kharakteristik ortotropnoy gladkoobolochechnoy modeli bikonicheskoy sektsii stvorki golovnogo obtekatelya* [Determination of stiffness and inertia-mass characteristics of an orthotropic smooth-shell model of the biconic section of the head cowl flap]. *Visnyk NTU «KhPI». Ser.:Transportne Mashynobuduvannia – Bulletin* of the *NTU 'KhPI'. Series*: *Transport Machine Building*, no.2 (71), pp. 39 – 46 [in Russian].
6. Tsybenko, A. S., Kryshchuk, N. H., Koniukhov, A. S., Koval, V. P., Aksonenko, A. V., & Trubin, A. V. (2006) *Rozrobka adekvatnoi matematychnoi modeli doslidzhennia dynamiky stulok holovnoho obtichnyka rakety-nosiia u protsesi polotu i viddilennia* [Development of an adequate mathematical model for studying the dynamics of the nose fairing flaps of a launch vehicle in flight process and separation]. *Nauk. visti NTU 'KhPI' – Science News of NTU 'KhPI'*, no. 6, pp. 139–148 [in Ukrainian].
7. Shulzhenko, N. G., Zaytsev, B. F., Asayenok, A. V., Protasova, T. V., Klimenko, D.V., Larionov, I. F., & Akimov, D. V. (2017). *Dinamika elementov sistemy otdeleniya obtekatelya rakety* [Dynamics of elements of the rocket fairing system]. *Aviats.-kosm. tekhnika i tekhnologiya – Aerospace Technic and Technology*, no. 9. (144), pp. 5–13 [in Russian].
8. Shulzhenko, N. G., Zaytsev, B. F., Asayenok, A. V., Klimenko, D. V., Batutina, T. Ya., & Burchakov, B. V. (2016). *Dinamicheskoye kontaktnoye vzaimodeystviye adapterov kosmicheskoy konstruktsii pri razdelenii* [Dynamic contact interaction of adapters of the space structure under separation]. *Aviats.-kosm. tekhnika i tekhnologiya – Aerospace Technic and Technology*, vol. 22, no. 2, pp. 12–21 [in Russian].
9. Shulzhenko, M. H., Zaitsev, B. P. , Hontarovskyi, P. P. , Protasova, T. V. , Batutina, T. Ya., & Sheremet, I. V. (2015). *Otsinka dynamichnoi reaktsii vuzliv systemy rozdilennia kosmichnoho aparata ta nosiia pry impulsnykh navantazhenniakh* [Estimation of the dynamic reaction of spacecraft and launch vehicle separation system units under pulse loads] *Kosm. nauka i tekhnolohiia – Space Science and Technology,* vol. 21, no. 1, pp. 15–19 [in Ukrainian].
10. Shulzhenko, N. G., Gontarovskiy, P. P., & Zaytsev, B. F. (2011). *Zadachi termoprochnosti, vibrodiagnostiki i resursa energoagregatov (modeli, metody, rezul'taty issledovaniy).* [Problems of thermal strength, vibrodiagnostics and resource of power units (models, methods, results of research): Monograph]. Saarbrücken, Germany: LAP LAMBERT Academic Publishing GmbH & Co. KG, 370 p. [in Russian].
11. Bate, K., & Vilson, Ye. (1982). *Chislennyye metody analiza i metod konechnykh elementov* [Numerical analysis methods and the finite element method]. Moscow: Stroyizdat, 448 p. [in Russian].
12. I.A. Birger & B.F. Shorr (Eds.). (1975). *Termoprochnost detaley mashin* [Thermal strength of machine parts. Moscow: Mashinostroyeniye, 455 p. [in Russian].
13. A.S Sakharov & I. Altenbach (Eds.). (1982). *Metod konechnykh elementov v mekhanike tverdykh tel* [The finite element method in the mechanics of solids). Kyiv: Vyshcha shkola, 480 p. [in Russian].
14. Timoshenko, S. P., & Gudyer, Dzh. (1975). *Teoriya uprugosti* [Theory of elasticity]. Moscow: Nauka, 576 p. [in Russian].

Received 16 May 2018

Динамічні процеси при ударній взаємодії елементів системи відділення обтічника ракети через пластичний демпфер

[1] Зайцев Б. П., [1] Асайонок О. В., [1] Протасова Т. В., [2] Клименко Д. В., [2] Акімов Д. В. , [2] Сіренко В. М.

[1] Інститут проблем машинобудування ім. А.М. Підгорного НАН України,
61046, Україна, м. Харків, вул. Пожарського, 2/10

[2] Державне підприємство «Конструкторське бюро «Південне» ім. М.К. Янгеля»,
49008, Україна, м. Дніпро, вул. Криворізька, 3

Статтю присвячено актуальним питанням забезпечення динамічної міцності елементів ракетної техніки під час використання піротехнічних засобів. Досліджується ударна взаємодія вузлів піротехнічної системи відділення обтічника ракети в другій фазі роботи системи за так званого «підхоплення». Контактування вузлів системи відбувається через пружно-пластичний демпфер. Демпфер встановлюється між рухомою та нерухомою частинами для «пом'якшення» удару за рахунок пластичної деформації. Демпфер виконує роль одностороннього зв'язку – обмежує стискання та не перешкоджає відриву. Приймається, що конструкція в цілому є пружною, а пластичне деформування зосереджене в демпфері. Механічна модель подається у вигляді комбінації пружних елементів й нелінійного демпфера. Методика врахування нелінійності демпфера побудована на введенні змінних граничних сил торцями демпфера. За пластичних деформацій стискання граничні сили збільшують деформацію, яка стримується пружними силами, а у разі порушення контакту – відриву – повністю компенсують напруження в моделі демпфера, занулюючи їх. Побудовано тривимірну розрахункову модель складеної конструкції обтічника в зборі. Демпфер подається у вигляді суцільного тонкого кільця. Використовується метод скінченних елементів. Розрахунок динаміки конструкції за часом виконується скінченно-різницевим методом Вільсона. Проведено верифікацію методики на тестовій задачі з відомим хвильовим розв'язком. Виконано розрахункові дослідження динамічного напруженого стану за деяких швидкостей удару для варіантів демпфера з різною пластичною жорсткістю: сталевого пружного (демпфер без отворів, «жорсткий», для порівняння); первинного (демпфер з отворами, пластичний, м'який) та раціонального (демпфер з підібраною характеристикою жорсткості). Показано, що первинний демпфер не є ефективним внаслідок недостатньої жорсткості. Визначені характеристики пластичної жорсткості, за яких динамічні напруження значно знижені відносно первинної конструкції. Максимальні динамічні напруження в піротехнічній системі відділення обтічника з раціональними демпферами сильно залежать від швидкості удару. За значних швидкостей вони перевищують границю пластичності. Більш точну постановку задачі «підхоплення» слід виконати з урахуванням пластичності у всій конструкції.

***Ключові слова**: обтічник, система відділення, удар, напруження, контакт, демпфер, пластичність.*

Література

1. Потапов А. М., Коваленко В. А., Кондратьев А. В. Сравнение головных обтекателей существующих и перспективных отечественных ракет-носителей и их зарубежных аналогов. *Авиац.-косм. техника и технология.* 2015. № 1 (118). С. 35–43.
2. Русин М. Ю., Ромашин А. Г., Камнев П. И. Опыт разработки головных обтекателей летательных аппаратов. *Авиац.-косм. техника и технология*. 2004. №5(13) . С. 63–69.
3. Моссаковский В. И., Макаренков А. Г., Никитин П. И., Саввин Ю. И. Прочность ракетных конструкций: учеб. пособие (под ред. В. И. Моссаковского). М.: Высш. шк., 1990. 359 с.
4. Колесников К. С., Кокушкин В. В., Борзых С. В., Панкова Н. В. Расчет и проектирование систем разделения ступеней ракет: учеб. пособие. М.: Изд-во МГТУ им. Н. Э. Баумана, 2006. 376 с.
5. Конюхов А.С. Определение жесткостных и инерционно-массовых характеристик ортотропной гладкооболочечной модели биконической секции створки головного обтекателя. *Вісн. НТУУ «КПІ»*. Сер. Машинобудування. 2014. №2 (71). С.39–46.
6. Цыбенко А. С., Крищук Н. Г., Конюхов А. С., Коваль В. П., Аксьоненко А. В., Трубін А. В. Розробка адекватної математичної моделі дослідження динаміки стулок головного обтічника ракети-носія у процесі польоту і відділення. *Наук. вісті НТУУ «КПІ»*. 2006. № 6. С.139–148.
7. Шульженко Н. Г., Зайцев Б. Ф., Асаенок А. В., Протасова Т. В., Клименко Д. .В.. Ларионов И. Ф., Акимов Д. В. Динамика элементов системы отделения обтекателя ракеты. *Авиац.-косм. техника и технология.* 2017. № 9. (144). С. 51–13.
8. Шульженко Н. Г., Зайцев Б. Ф., Асаенок А. В., Клименко Д. В., Батутина Т. Я., Бурчаков Б. В. Динамическое контактное взаимодействие адаптеров космической конструкции при разделении. *Косм. наука і технологія.* 2016. Т .22. № 2. С. 12–21.
9. Шульженко М. Г., Зайцев Б. П. , Гонтаровський П. П. , Протасова Т. В. , Батутіна Т. Я. , Шеремет І. В. Оцінка динамічної реакції вузлів системи розділення космічного апарата та носія при імпульсних навантаженнях. *Косм. наука і технологія.* 2015. Т. 21. № 1. С. 15–19.
10. Шульженко Н. Г., Гонтаровский П. П., Зайцев Б. Ф. Задачи термопрочности, вибродиагностики и ресурса энергоагрегатов (модели, методы, результаты исследований): моногр. Saarbrücken, Germany: LAP LAMBERT Academic Publishing GmbH & Co.KG, 2011. 370 с.
11. Бате К., Вильсон Е. Численные методы анализа и метод конечных элементов. М.: Стройиздат, 1982. 448 с.
12. Термопрочность деталей машин (под ред. И.А. Биргера и Б.Ф. Шорра). М.: Машиностроение, 1975. 455 с.
13. Метод конечных элементов в механике твердых тел (под общ. ред. А. С. Сахарова и И. Альтенбаха). Киев: Вища шк., 1982. 480 с.
14. Тимошенко С. П., Гудьер Дж. Теория упругости. М.: Наука, 1975. 576 с.